LOCAL TUNING BIASES IN MOUSE LATERAL GENICULATE NUCLEUS

INTRODUCTION

INTRODUCTION

Simple cells in the primary visual cortex (V1) are selective to multiple properties of images, most notably the location and orientation of edge-like features within a local region [1] . Neurons with these orientation tuned responses are present in V1 of all known mammals [2] suggesting that they are fundamental for visual processing [2].

Despite the importance and decades of research into the topic, the mechanism that generates tuning remains an open question. Part of the debate regards how orientation tuning is generated in *individual* simple cells, and how this mechanism relates to the process that generates the organization of tuned cortical *populations* [3]. For example, in higher mammals, vertical columns of cells show similar orientation preferences, and the preference of these columns rotates smoothly, in a quasiperiodic fashion, as one moves horizontally across the cortex [1,4]. However, in V1 of the mouse, neurons have larger receptive fields, and cells with different tuning preferences are scattered randomly across the cortical tissue [5]. Despite these variations across species the general structure of the spatial receptive fields (RFs) and the orientation selectivity of simple cells remains constant [6].

Another open question is whether the process that generates tuning in mouse V1 is similar to the process that generates the tuning of neurons in the mouse dorsal lateral geniculate nucleus (dLGN). The mouse retina is populated by a subclass of retinal ganglion cells (RGCs) that respond robustly to stimulus movement along one of the cardinal directions [7] . The mouse dLGN also contains these cardinal-direction tuned cells and, in addition, is populated by cells that are selective to both directions that form an axis (e.g., both upward *and* downward motion) [8,9] . In all, these observations pose a challenge to models which must explain how or if orientation

tuning in V1 is implemented in a similar fashion across different species and across different visual regions [10].

TUNING VS RETINOTOPY

A family of models, inspired by the work of Hubel and Wiesel [1] suggest that the feedforward convergence of ON and OFF signals onto cortical population of cells endows them with their orientation tuning. These models make predictions regarding the relationship between orientation tuning of neurons and their spatial receptive fields [11-13]. One particular model posits that cells representing the same local image regions have similar tuning preference [13-15]. A myriad of recent studies of local populations of cells in mouse V1 corroborate this notion. In mouse V1, cells with overlapping RFs have highly correlated activity over long periods of stimulation [16,17] and, in turn, cells with such strong correlations tend to have similar orientation preferences [17]. Furthermore, V1 neurons with similar RFs are likely to be strongly bidirectionally connected, and these strongly wired cells tend to share orientation preferences [16,18,19]. Excitatory connected V1 neurons, known share similar orientation preferences [18], are also driven by the same thalamic afferent [20], perhaps because they are driven by signals from a similar region of visual space.

More evidence that local retinal regions are represented by a biased set of tuned cells comes from studies of 'sibling' neurons (i.e., clonally related cells derived from the same progenitor cell). Sibling neurons are connected via electrical junctions early in development causing them to form strong chemical synapses and similar tuning preferences in adulthood [21-24]. In an effort to simulate the development of these sibling cells, Ko and colleagues [19] designed a neural network of cells that, prior to training, were connected via these electrical junctions. During training, sibling cells acquired highly similar RFs leading to two consequences: The activity of siblings became highly correlated, and they developed strong bilateral connections, both of which are traits of cells that are tuned to the same orientation [16,18,19,21-24]. Thus, the developmental model suggests that sibling neurons with similar RFs are destined to acquire similar tuning preferences. Furthermore, a recent pair of studies revealed that mouse superior colliculus (SC) contains vertical columns of cells with similar orientation preferences, but each of these columns only cover a specific portion of the visual field which do not overlap with the RFs of other columns [25,26]. In conclusion, studies of multilaminar V1 networks, among others [20,27], support the notion that cells representing the same point of visual space are constrained to have the same tuning preference.

THE CURRENT STUDY

Recently, we found more evidence of local tuning biases in mouse V1, such that cells that have overlapping ON or OFF subregions have similar orientation and spatial frequency tuning [14]. The source of these local tuning biases remains an open question. One idea is that they are inherited from the thalamus, and possibly, that the thalamus inherits its local tuning biases from the retina (**Figure 3**). Here we assess whether such local tuning biases exist the mouse dLGN, known to contain direction, axis, and spatial frequency tuned neurons [8,9,28-31] which project tuned afferents [32,33] to V1. Using in vivo-two photon imaging, we estimated the linear spatial RF maps and joint orientation and spatial frequency tuning of thalamic afferents innervating mouse V1. We find a significant relationship between the RF overlap and tuning similarity of these geniculate inputs. Our findings corroborate the notion that local tuning biases of thalamic afferents originate from the retina and are relayed onto the V1, preventing cortical populations from representing local regions of visual space with a diverse set of tuning profiles [34].

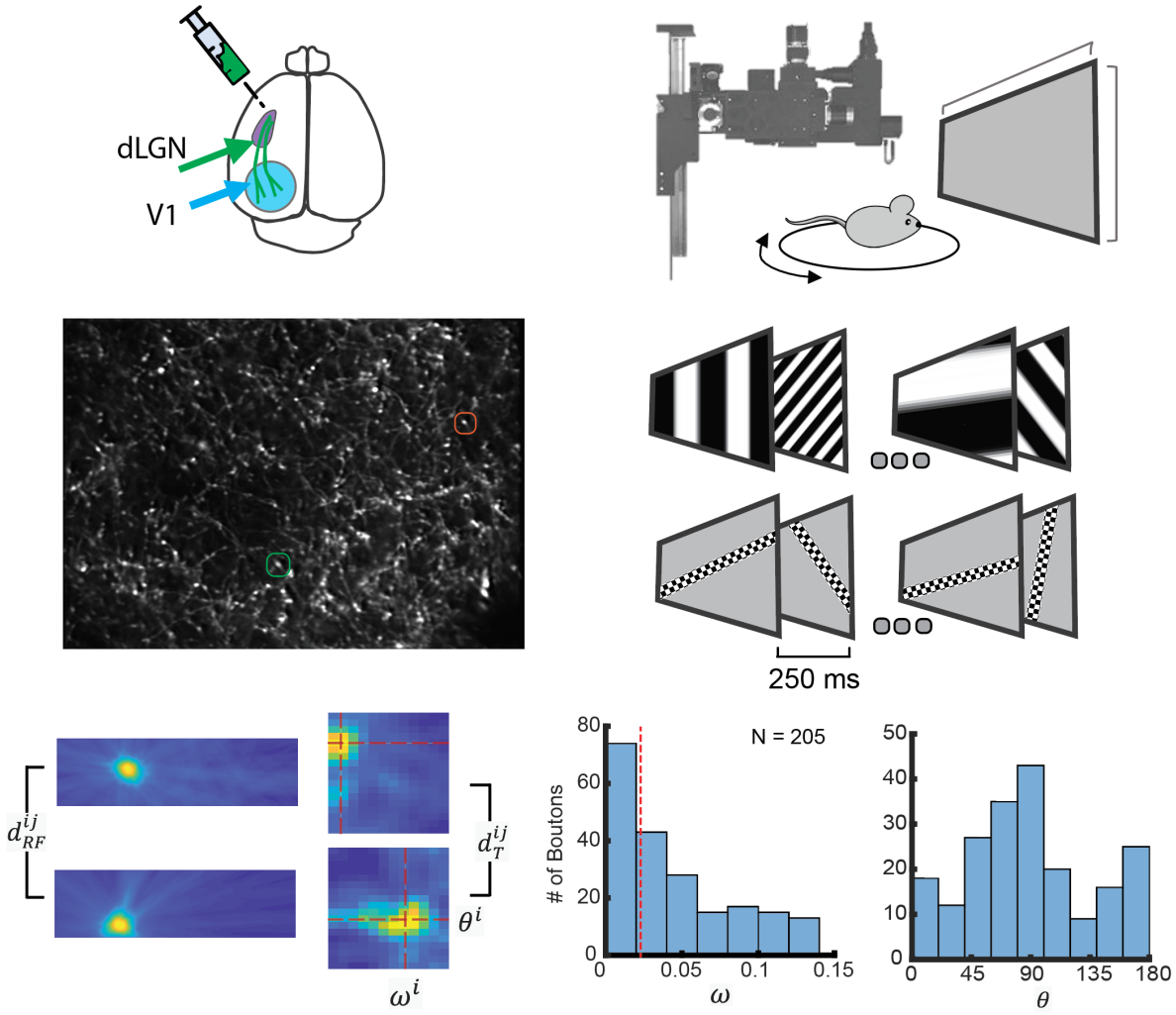

FIGURE 1 TUNING, RF MAPS, AND THEIR SIMILARITIES, OF DLGN BOUTONS.

(A, top) *Injection of GcaMP6s in the dLGN using an AAV leads to expression in thalamic afferents innervating V1.* ***(A, bottom)*** *Example snapshot of a population of GcaMP6s expressing boutons innervating mouse V1.*
(B) *In vivo two-photon calcium imaging of dLGN afferents in V1 during visual stimulation. Mice are head-restrained but otherwise free to walk, rest, or groom on a spherical treadmill while viewing stimuli shown in (C).*
(C, Top) *Pseudorandom sequences of full-field sinusoidal gratings were used to map the tuning of boutons for orientation and spatial frequency.* ***(C, Bottom)*** *To estimate RF maps of boutons, a sequence of elongated bars were flashed at different locations and orientations across the screen.*
(D) *Example of RF maps, joint tuning kernels and their similarities for two dLGN boutons, i and j, from the same imaging field shown in (A, bottom). Maps and kernels are normalized and presented in arbitrary units. The overlap between RF maps and similarity of tuning kernels, between two boutons i and j is denoted by* d_{RF}^{ij} *and* d_T^{ij}*, respectively. For each bouton, the preferred orientation of the cell,* θ_i*, and its preferred spatial frequency,* ω_i*, is taken from the peak of the tuning kernel.*
*(**E, left**) Histogram of spatial frequency preferences of dLGN boutons with significant tuning kernels. Red vertical line denotes the median value of 0.028 cycles per degree.* ***(E, right)*** *Histogram of preferred orientations preferences of dLGN boutons with significant tuning kernels. There is a strong bias towards cardinal orientations*

RESULTS

We expressed GcaMP6s in dLGN boutons innervating L2/3 and L4 of mouse primary visual cortex and measured their visual properties using resonant, two-photon microscopy in the awake, behaving mouse (**Figure 1**).

A bouton's joint tuning to orientation and spatial frequency was measured by presenting a sequence of flashed, high-contrast sinusoidal gratings having pseudorandom orientations and spatial frequencies (**Figure 1**). We estimated the tuning of each bouton by linearly regressing its response on the grating stimulus and denote the estimated tuning kernel of the ith bouton in an imaging field by H_T^i. The peak of the tuning kernel also yielded a spatial frequency preference ω_i and an orientation preference θ_i for each bouton (see methods, **Figure 1**).

We also measured the spatial receptive field maps of boutons by presenting a sequence of flickering, elongated bars at random orientations and positions across the visual field (**Figure 1**). A boutons RF map was estimated by correlating its response and the location of the bars. We denote the RF map corresponding to the ith bouton in an imaging field by H_R^i.

We find that dLGN boutons innervating mouse primary visual cortex are orientation and spatial frequency selective and the distribution of preferred orientations has a bias for cardinal orientations. (**Figure 1).**

To assess the existence of local tuning biases of dLGN inputs to mouse V1, we asked if boutons with overlapping RFs have similar joint tuning profiles. We define the tuning similarity of bouton pairs as the as the correlation between their joint tuning kernels $d_T^{ij} = \langle H_T^i, H_T^j \rangle / \|H_T^i\| \|H_T^j\|$. The RF overlap of bouton pairs is defined as the correlation coefficient between their RF maps $d_R^{ij} = \langle H_R^i, H_R^j \rangle / \|H_R^i\| \|H_R^j\|$. We find a significant positive correlation between the joint tuning similarity of bouton pairs and the overlap between their RFs (r = 0.29, p=9.5 x 10^{-5}, n = 178) (**Figure 2**).

As a further test, we assessed the distribution of joint tuning similarity of boutons with high RF overlap and compared to those with low RF overlap. Bouton pairs with RF correlations that fell within the first and fourth quartile of the RF correlation distribution were deemed to have RFs with high and low overlap, respectively (**Figure 2**). The joint tuning similarity of boutons with high RF overlap was significantly greater than those with low RF overlap (median d_T^{ij} with high RF overlap = 0.79, median d_T^{ij} with low RF overlap = 0.28, Wilcoxon ranked-sum 2-tailed test, P= 7 x 10^{-6} ; (**Figure 2**). Both scatter plots shown in (**Figure 2**) and have regression lines that are bounded by a 95% confidence interval. The left vertical line and right vertical lines of the scatter plots denote the 25th and 75th percentile of the RF correlation distribution, respectively.

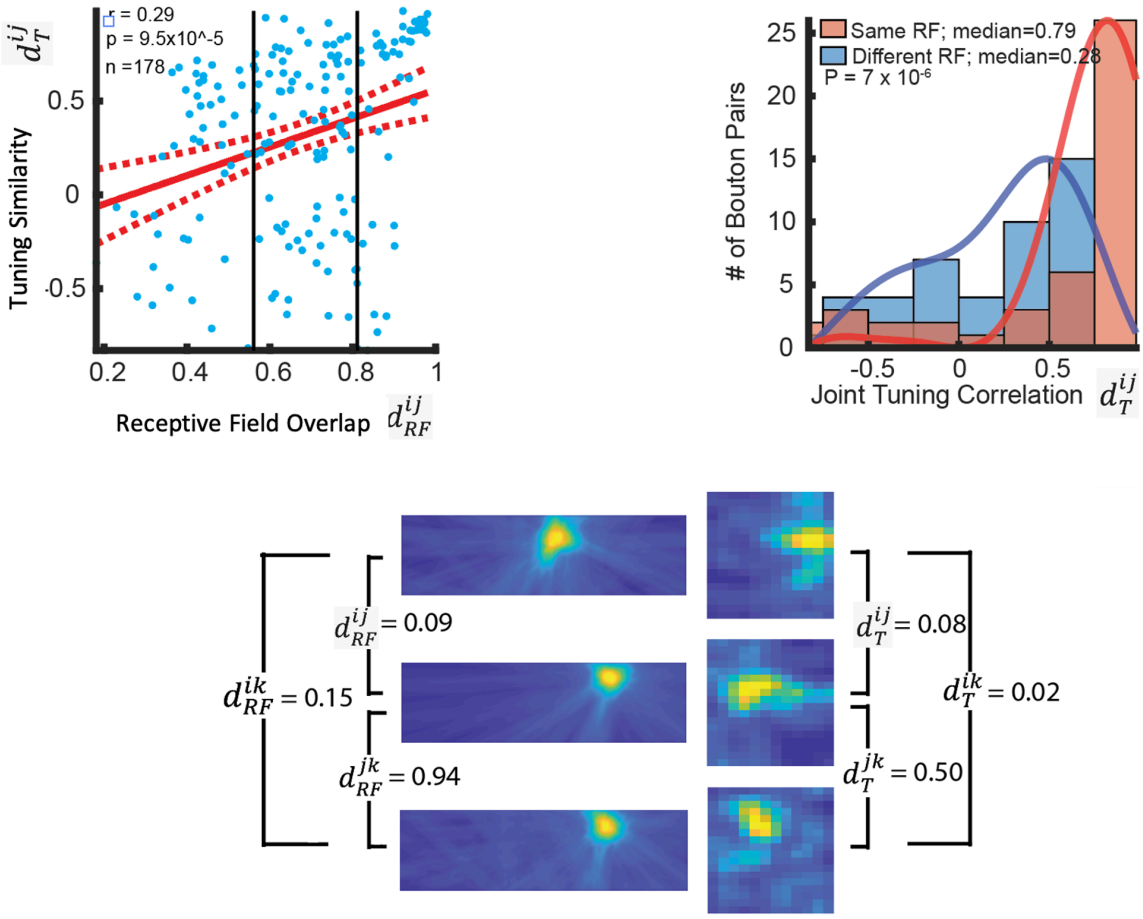

FIGURE 2 EVIDENCE OF LOCAL TUNING BIASES IN DLGN BOUTONS INNERVATING MOUSE V1

(Top left) *Scatter plot and fitted regression line showing a positive correlation between tuning similarity and RF overlap, for all boutons in the data set (5 fields, 3 mice total).*

(Top right) *Histogram of joint tuning similarity for bouton pairs with overlapping (blue) and non-overlapping (red) RFs. Bouton pairs with overlapping RF (red) have a significantly higher tuning similarity (Median = 0.34) than those with different RFs (Median = 0.21)*

(Bottom) *RFs maps (left column) and tuning kernels (right column) for three boutons I (top row), j (middle row) and k (bottom row) from the same imaging session. Middle and bottom boutons, j and k, have overlapping receptive fields and similar tuning. The top bouton, i, has a different RF and different tuning kernel than those of boutons j and k.*

DISCUSSION

We find that individual thalamic afferents are slightly less selective compared to the outputs of cortical cells **(Figure 1),** as reported in another study [32] (although see reference [33]). Our main finding is that thalamocortical afferents with overlapping RFs do not have a diverse set of tuning profiles and are instead biased towards a specific orientation and spatial frequency. These biases resemble the local tuning biases observed in V1 we reported in an earlier study [14], where cells with overlapping RFs have similar tuning profiles. These results suggests that local tuning biases in mouse V1 can be inherited from biases in their thalamic inputs.

There are at least three mechanisms that can explain the local tuning biases observed in the primary visual cortex and thalamic afferents. Thalamic neurons may acquire their similar and overlapping RFs if they all combine the inputs from the same spatially neighboring pair of ON and OFF center RGCs (**Figure 3A**), or if they all are driven by the same direction tuned RGC (**Figure 3 B**). In both of these scenarios, thalamic cells or cortical cells with overlapping RFs would have similar tuning. A third scenario is that untuned center surround thalamic cells with spatially offset ON- and OFF- subregions converge onto multiple cortical targets, endowing them with the same tuning preference and similar receptive fields (**Figure 3C**)

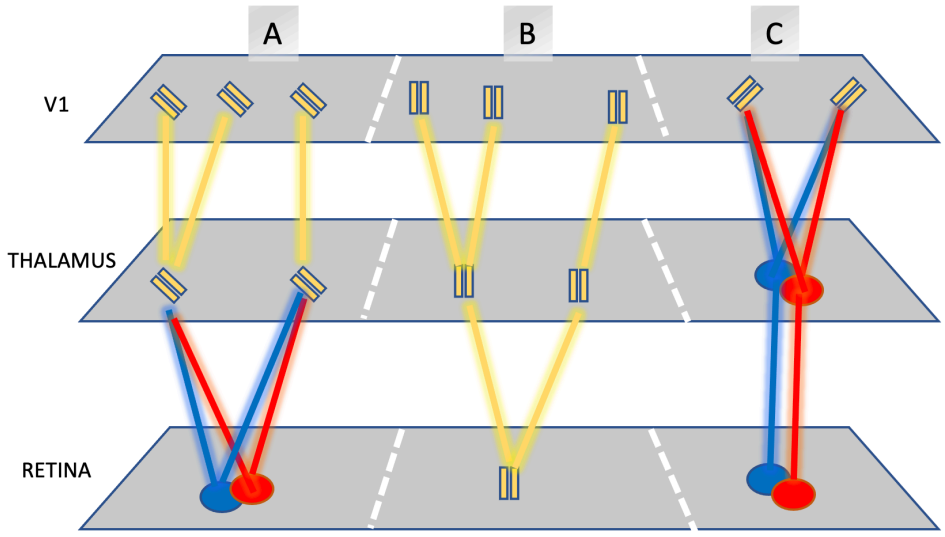

FIGURE 3 THREE POSSIBLE MECHANISMS THAT GENERATE LOCAL TUNING BIASES IN THALAMIC AFFERENTS OR THEIR CORTICAL TARGETS

(A) *Thalamic cells acquire similar tuning (i.e., show local tuning biases) by receiving convergent input from a pair of neighboring ON- and OFF- center RGCs. In turn, these thalamic cells project their tuned afferents and innervate multiple cortical cells.*
(B) *A direction tuned RGC endows its thalamic targets with a similar direction preference direction, and these thalamic neurons relay the same tuned signal onto multiple cortical targets.*
(C) *A the axons of a pair untuned thalamic cells with spatially offset ON- and OFF subfields converge onto multiple cortical cells.*
In mechanism A and B, but not C, thalamic afferents could also exhibit local tuning biases. In all three cases, cortical simple cells will exhibit local tuning biases.

ORIENTATION TUNING OF SINGLE CELLS IN THE DLGN

Assuming the different thalamic afferents we measured belonged to different thalamic cells, our results show that thalamic neurons with similar RFs are likely to have similar tuning. This suggests that the dLGN also represents local image regions with a biased set of orientation tuned cells, similar to recent findings of the mouse SC [25,26]. Why would groups of dLGN cells pooling inputs from the same retinal region have similar tuning preferences?

Traditionally, the thalamus is said to lack cells that are tuned to stimulus orientation [3,4,35]. In mice however, this is clearly not the case. Some neurons in the dLGN, especially those in the shell region **(**Error! Reference source not found.), are clearly tuned [8,30,33,36-38], either to movement along a single direction (e.g., the upward movement only), or along an axis (e.g., both upward *and* downward movement) [8,9,29-33,36,38].

INHERITANCE OF TUNING FROM THE RETINA

Causal evidence supports the notion that cells in the mouse SC directly inherit their tuning from RGCs selective to motion along the one of the cardinal directions [39]. These findings have inspired the idea that direction tuned dLGN cells also acquire their tuning from direction selective RGC inputs [29,33,35,40] (**Figure 3 B**). Similarly, axis selectivity in the dLGN is proposed to emerge from the thalamic pooling of RGC inputs that are tuned to opposite motion directions [9,35,38,41].

However, models of dLGN tuning that invoke the pooling of direction tuned RGCs face some challenges. For instance, orientation tuning in mouse V1 remains relatively intact in transgenic mouse lines with deficits in retinal directional selectivity [42], suggesting that tuning in the dLGN does not depend on direction tuned inputs from the retina.

Moreover, it is not clear how thalamic cells that are tuned to a *single direction* avoid combining a large number of diverse inputs tuned to multiple directions. Promiscuous pooling of a large number of diverse inputs would likely preclude orientation selectivity of dLGN neurons. This is problem evident in inhibitory V1 neurons which are poorly selective due to pooling the inputs of neurons with a diversity of tuning preferences [43].

Similarly, it is not known how dLGN cells tuned to a specific *axis* of motion can specifically 'pick and choose' RGCs with opposite motion preferences. Even if axis selective dLGN neurons are able to specifically pool only from RGC inputs with opposing motion preferences (see reference [9]), it is not clear how their tuning would remain sharp given that these motion signals conflict and can 'cancel' each other out. For instance, human psychophysical experiments show that motion percepts are lost when observers view stimuli moving in opposite direction within in local visual regions [44].

POOLING OF ON/OFF RGCS

Another possibility is that that tuning in the dLGN is generated de-novo, for example, dLGN neurons can their tuning by pooling from spatially displaced ON- and OFF center surround RGCs [45,46] (**Figure 3 A**).

Direction Tuning

Direction tuning in the dLGN can emerge via a Reichardt type mechanism, in which a dLGN neuron pools from center-surround RGCs with side-by-side RFs and different temporal dynamics. This is a plausible mechanism given that center surround RGCs, with transient and sustained responses [7,47], form the majority of axons that that project to the dLGN [8] . Moreover, these Reichardt computations are implemented by the bipolar-to-amacrine retinal network across the animal kingdom [48-50] and can possibly explain how layer 4 neurons in mouse V1 acquire their direction tuning [51].

Axis Tuning

Axis tuning in the dLGN can also be accomplished if a dLGN neuron pools from a pair of spatially offset, center-surround RGCs with the same temporal response pattern. A dLGN neuron that combines such inputs would show robust responses to stimuli moving in both opposing motion directions that form an axis [46]. This idea consistent with findings showing that the responses of some dLGN neurons to the orientation of gratings can be predicted by the orientation of their RFs, although with considerable error [10,30,31] .

LIMITED INPUT

Regardless of how direction or axis tuning emerges, a unresolved question is exactly how thalamic cells 'pick and choose' an appropriate set of retinal inputs. If dLGN cells inherit their direction or axis tuning from direction tuned RGCs, how do they avoid combining a too many RGCs tuned to a diverse set of directions? Or if dLGN neurons acquire their tuning by combining the inputs of neighboring ON- and OFF center surround cells , how do they avoid selecting inputs with largely separate RFs? One explanation is that thalamic neurons are compelled to select an appropriate set of RGCs, simply because the number of RGC inputs available to them is limited. Restricting the size of the retinal input pool would effectively constrain the diversity tuning profiles a thalamic cell can build [45,52] (Error! Reference source not found.). If dLGN cells are given only a few inputs to choose from, they will be less likely to pool a diverse range of different motion signals, or pool center surround inputs with inappropriately arranged RFs. Indeed, a random wiring model that assumes that inputs are limited [9] appears to explain the emergence of direction and axis tuning in the dLGN [9]. Moreover, a limited input scenario is expected to endow postsynaptic cells with overlapping RFs with similar tuning, consistent with the local tuning biases we observed here and those observed in the SC [25,26].

CONCLUSION

Note that we did not estimate the ON- or OFF- subregions of thalamic afferents. Therefore, we are not able to determine if local tuning biases in mouse V1 could emerge due to the convergence of center surround, untuned inputs (**Figure 3 C**).. However, there is developing evidence that thalamic afferents with spatially offset subregions or different temporal response patterns converge onto a common cortical cell to endow it with axis [46] or direction [51] tuning.

Another drawback is our inability to ensure that thalamic boutons originated from different thalamic cells. Although this was an issue, note that the RF maps of afferents, as well as their tuning kernels, showed great diversity (**Figure 2**). Also consider that in mice, there is a relatively large number of distinct thalamic axons that target the same cortical region (5000 afferents/mm2)[53]. It is therefore likely that we imaged thalamocortical afferents belonging to a large number of thalamic cells.

Finally, note that the correlation between RF overlap and tuning similarity is slightly weaker in the dLGN afferents than that we observed in V1 [14] (r = 0.29 in dLGN, r=0.38 in V1). Moreover, we also find that pairs of boutons with overlapping RFs also tend to show different degrees of tuning similarity (**Figure 2)**. Despite these drawbacks the fact that we find a significant trend suggests that local tuning biases in thalamocortical inputs to mouse V1 may indeed exist.

Similar to our findings, two recent studies of the mouse SC demonstrate that cells representing the same region of visual space have the same preference towards motion along a specific axis [25,26]. These findings, together with our results, suggest that local tuning biases in the thalamocortical network originate from the biases in the local arrangement of retinal ganglion cells [13].

METHODS

Animals

All procedures were approved by the University of California, Los Angeles, Office of Animal Research Oversight (the Institutional Animal Care and Use Committee) and were in accord with guidelines set by the US National Institutes of Health. A total of three C57BL/6J mice (The Jackson Laboratory), were used in this study. Mice were housed in groups of 2 or 3, in reversed light cycle. Animals were naïve subjects with no prior history of participation in research studies. We imaged **[9]** different fields to obtain the data discussed in this paper.

Surgery

Carprofen and buprenorphine analgesia were administered preoperatively. Mice were then anesthetized with isoflurane (4–5% induction; 1.5–2% surgery). Core body temperature was maintained at 37.5°C using a feedback heating system. Eyes were coated with a thin layer of ophthalmic ointment to prevent desiccation. Anesthetized mice were mounted in a stereotaxic apparatus. Blunt ear bars were placed in the external auditory meatus to immobilize the head. A portion of the scalp overlying the two hemispheres of the cortex (~8 x 6 mm) was then removed to expose the underlying skull. After the skull was exposed, it was dried and covered by a thin layer of Vetbond. After the Vetbond dried (~15 min), it provided a stable and solid surface to affix the aluminum bracket with dental acrylic. The bracket was then affixed to the skull, and the margins were sealed with Vetbond and dental acrylic to prevent infections.

Virus Injection

We followed a similar procedure for virus injection to express GcaMP6f in LGN axons described elsewhere [32,54] . A 3-mm-diameter region of skull overlying the occipital cortex was removed. Care was taken to leave the dura intact. GcaMP6-slow was expressed in the dorsal lateral geniculate nucleus (dLGN) using adeno-associated virus. AAV-GcaMP6-slow was loaded into a glass micropipette and slowly inserted into the dLGN using a micromanipulator. AAV-GcaMP6-slow was pressure-injected using a Picospritzer. The injections were made by a computer program in control of the micromanipulator and the Picospritzer.

A sterile 3-mm-diameter cover glass was then placed directly on the dura and sealed at its edges with Vetbond. When dry, the edges of the cover glass were further sealed with dental acrylic. At the end of the surgery, all exposed skull and wound margins were sealed with Vetbond and dental acrylic, and a small, sealed glass window was left in place over the occipital cortex. The mouse was then removed from the stereotaxic apparatus, given a subcutaneous bolus of warm sterile saline, and allowed to recover on the heating pad. When fully alert, it was placed back in its home cage.

Imaging

Once expression of GcaMP was observed in thalamic boutons within the layers of primary visual cortex, typically between 2 to 3 weeks after the injection, imaging sessions took place. Imaging was performed using a resonant, two-photon microscope (Neurolabware, Los Angeles, CA) controlled by Scanbox acquisition software (Los Angeles, CA). The light source was a Coherent Chameleon Ultra II laser (Santa Clara, CA) running at 920 nm. The objective was a □16 water immersion lens (0.8 numerical aperture, 3-mm working distance; Nikon). The microscope frame rate was 15.6 Hz (512 lines with a resonant mirror at 8 kHz). Eye movements and pupil size were recorded via a Dalsa Genie M1280 camera (Teledyne Dalsa) fitted with a 740-nm long-pass filter that looked at the eye indirectly through the reflection of an infrared- reflecting glass.

Visual stimulation

Sequences of pseudorandom sinusoidal gratings [55,56] and checkered bars were generated in real-time by a Processing sketch using OpenGL shaders (see https://processing.org) on a wide screen spanning 100 x 55 in degrees and refreshed at 60 Hz.

In generating pseudo-random gratings, the orientation domain was sampled in equal steps of 10° for a total of 18 possible orientations; the spatial frequency domain was sampled in equal steps on a logarithmic scale from 0.0079 to 0.1549 cycles/°, for a total of 12 possible spatial frequencies; and for each combination of orientation and spatial frequency, spatial phase was equally sampled in steps of 45°, leading to a total of 8 possible settings. The tuning kernels (see *Kernel Estimation*) were computed by averaging responses over spatial phase, as done in previous studies (Malone and Ringach 2008; Ringach et al. 2002). The duration of the sequences was 20 min, and gratings were updated 4 times a second.

To estimate the locations of the receptive fields an elongated bar, composed of a flickering checkerboard pattern, was briefly presented at a random location and orientation on the screen. Bar were replaced with a different bar with a random position and angle 4 times per second. The bars always spanned the entire screen and were 10 degrees wide. The total duration of the stimulus was 25 minutes.

Transistor-transistor logic signals generated by the stimulus computer were sampled by the microscope and time-stamped with the frame and line number being scanned at that time. The timestamps provided the synchronization between visual stimulation and imaging data.

In all experiments, we used a Samsung CHG90 monitor viewed at 20-cm distance. The screen was calibrated using a Photo Research (Chatsworth, CA) PR-650 spectroradiometer, and the result was used to generate the appropriate -corrections for the red, green, and blue components via an NVIDIA Quadro K4000 graphics card. The contrast of the stimulus was 80%. The center of the monitor was positioned with the center of the receptive field population for the eye

contralateral to the cortical hemisphere under consideration. We imaged the monocular region of V1 in the left hemisphere.

Image processing

The image processing pipeline was the similar to that described in detail elsewhere [57] . Briefly, calcium images were aligned to correct for motion artifacts. Following motion stabilization, we used a MATLAB (MathWorks, Natick, MA) graphical user interface tool developed in our laboratory to define regions of interest manually. These regions corresponded micrometer-sized circular or elliptical boutons of dLGN axons. Following segmentation, we extracted signals by computing the mean of the calcium fluorescence within each region of interest and discounting the signals from the nearby neuropil. Spikes were then estimated via deconvolution [58]

Estimation of Kernels

The estimation of a tuning kernel was performed by fitting a linear model between the inferred spiking response of a bouton and the grating stimulus at multiple time lags [57] (Jimenez 2018). Similarly, we computed the retinotopic map of a bouton by fitting a time lagged linear model between the response and the location of bars.

We used bouton kernels at their optimal time delay between the stimulus and response. The optimal delay for a tuning kernel was defined as the time at which the variance of the kernel reached its maximum. A tuning kernel was defined as significant if the peak variance was at least 1.75 times that of the baseline measured at negative time lags.

We defined the optimal delay time for the retinotopic map as the one at which the map's kurtosis reached its maximum. RF maps were deemed significant if their kurtosis value exceeded a value of 13. This kurtosis threshold assured that only RFs highly localized peaks were included. These optimal retinotopic map were then smoothed with the Gaussian window of 5 degrees of visual space. The results presented here use data from boutons with significant tuning kernels and significant retinotopic maps.

We denote the estimated tuning kernel and retinotopic kernel of the i-th bouton in an imaging field by H_T^i and H_{RF}^i, respectively.

Estimation of orientation and spatial frequency preference

We also denote the preferred spatial frequency of the ith bouton as ω^i, defined as the center of mass of the horizontal slice of the tuning kernel passing through the peak response (Error! Reference source not found.). Similarly, we denote the preferred orientation of each bouton as θ^i, defined as the center of mass of the vertical slice of the tuning kernel passing through the peak response (Error! Reference source not found.).

Tuning similarity and RF overlap

We defined joint tuning similarity of bouton pairs as the correlation coefficient between their joint tuning kernels.

$$d_T^{ij} = \frac{\langle H_T^i, H_T^j \rangle}{\|H_T^i\| \|H_T^j\|}$$

We defined the overlap of the receptive fields of pairs of boutons as the correlation coefficient between their receptive field maps.

$$d_{RF}^{jk} = \frac{\langle H_{RF}^{i}, H_{RF}^{j} \rangle}{\left\| H_{RF}^{i} \right\| \left\| H_{RF}^{j} \right\|}$$

For Wilcoxin rank-sum tests, we assessed tuning similarity for boutons with RFs showing high overlap and those with low overlap. Bouton pairs were deemed to have high RF overlap if the correlation between their RFs fell within the upper quartile of the population RF correlation distribution. Boutons were deemed to low RFs overlap if their correlations fell in the lower quartile of the population RF distribution.

REFERENCES

1 Hubel, D. H. & Wiesel, T. N. Ferrier lecture - Functional architecture of macaque monkey visual cortex. *Proceedings of the Royal Society of London. Series B. Biological Sciences* **198**, 1-59, doi:10.1098/rspb.1977.0085 PMID - 20635 (1977).

2 Van Hooser, S. D. Similarity and Diversity in Visual Cortex: Is There a Unifying Theory of Cortical Computation? *The Neuroscientist* **13**, 639-656, doi:10.1177/1073858407306597 (2007).

3 Vidyasagar, T. R. & Eysel, U. T. Origins of feature selectivities and maps in the mammalian primary visual cortex. *Trends in Neurosciences* **38**, 475-485, doi:10.1016/j.tins.2015.06.003 (2015).

4 Hubel, D. H. & Wiesel, T. N. Receptive fields, binocular interaction and functional architecture in the cat's visual cortex. *The Journal of Physiology* **160**, 106-154, doi:10.1113/jphysiol.1962.sp006837 PMID - 14449617 (1962).

5 Ohki, K., Chung, S., Ch'ng, Y. H., Kara, P. & Reid, R. C. Functional imaging with cellular resolution reveals precise micro-architecture in visual cortex. *Nature* **433**, 597-603, doi:10.1038/nature03274 (2005).

6 Niell, C. M. & Stryker, M. P. Highly Selective Receptive Fields in Mouse Visual Cortex. *The Journal of Neuroscience* **28**, 7520-7536, doi:10.1523/jneurosci.0623-08.2008 PMID - 18650330 (2008).

7 Baden, T. *et al.* The functional diversity of retinal ganglion cells in the mouse. *Nature* **529**, 345-350, doi:10.1038/nature16468 PMID - 26735013 (2016).

8 Piscopo, D. M., El-Danaf, R. N., Huberman, A. D. & Niell, C. M. Diverse Visual Features Encoded in Mouse Lateral Geniculate Nucleus. *Journal of Neuroscience* **33**, 4642-4656, doi:10.1523/JNEUROSCI.5187-12.2013 (2013).

9 Marshel, J. H., Kaye, A. P., Nauhaus, I. & Callaway, E. M. Anterior-Posterior Direction Opponency in the Superficial Mouse Lateral Geniculate Nucleus. *Neuron* **76**, 713-720, doi:10.1016/j.neuron.2012.09.021 (2012).

10 Scholl, B., Tan, A. Y. Y., Corey, J. & Priebe, N. J. Emergence of Orientation Selectivity in the Mammalian Visual Pathway. *The Journal of Neuroscience* **33**, 10616-10624, doi:10.1523/jneurosci.0404-13.2013 PMID - 23804085 (2013).

11 Kremkow, J. & Alonso, J.-M. Thalamocortical Circuits and Functional Architecture. (2018).

12 Paik, S. B. & Ringach, D. L. Link between orientation and retinotopic maps in primary visual cortex. *Proceedings of the National Academy of Sciences of the United States of America* **109**, 7091-7096, doi:10.1073/pnas.1118926109 (2012).

13 Paik, S. B. & Ringach, D. L. Retinal origin of orientation maps in visual cortex. *Nature Neuroscience* **14**, 919-925, doi:10.1038/nn.2824 (2011).

14 Jimenez, L. O., Tring, E., Trachtenberg, J. T. & Ringach, D. L. Local tuning biases in mouse primary visual cortex. *Journal of Neurophysiology* **120**, 274-280, doi:10.1152/jn.00150.2018 PMID - 29668380 (2018).

15 Ringach, D. L. On the origin of the functional architecture of the cortex. *PLoS ONE* **2**, doi:10.1371/journal.pone.0000251 (2007).

16 Ko, H. *et al.* Functional specificity of local synaptic connections in neocortical networks. *Nature* **473**, 87-91, doi:10.1038/nature09880 (2011).

17 Bonin, V., Histed, M. H., Yurgenson, S. & Reid, R. C. Local diversity and fine-scale organization of receptive fields in mouse visual cortex. *Journal of Neuroscience* **31**, 18506-18521, doi:10.1523/JNEUROSCI.2974-11.2011 (2011).

18 Cossell, L. *et al.* Functional organization of excitatory synaptic strength in primary visual cortex. *Nature* **518**, 399-403, doi:10.1038/nature14182 PMID - 25652823 (2015).

19 Ko, H. *et al.* The emergence of functional microcircuits in visual cortex. *Nature* **496**, 96-100, doi:10.1038/nature12015 (2013).

20 Morgenstern, N. A., Bourg, J. & Petreanu, L. Multilaminar networks of cortical neurons integrate common inputs from sensory thalamus. *Nature Neuroscience* **19**, 1034-1040, doi:10.1038/nn.4339 PMID - 27376765 (2016).

21 Ohtsuki, G. *et al.* Similarity of visual selectivity among clonally related neurons in visual cortex. *Neuron* **75**, 65-72, doi:10.1016/j.neuron.2012.05.023 (2012).

22 Li, Y. *et al.* Clonally related visual cortical neurons show similar stimulus feature selectivity. *Nature* **486**, 118-121, doi:10.1038/nature11110 (2012).

23 Yu, Y. C. *et al.* Preferential electrical coupling regulates neocortical lineage-dependent microcircuit assembly. *Nature* **486**, 113-117, doi:10.1038/nature10958 (2012).

24 Yu, Y. C., Bultje, R. S., Wang, X. & Shi, S. H. Specific synapses develop preferentially among sister excitatory neurons in the neocortex. *Nature* **458**, 501-504, doi:10.1038/nature07722 (2009).

25 Ahmadlou, M. & Heimel, J. A. Preference for concentric orientations in the mouse superior colliculus. *Nature Communications* **6**, 6773, doi:10.1038/ncomms7773 PMID - 25832803 (2015).

26 Feinberg, E. H. & Meister, M. Orientation columns in the mouse superior colliculus. *Nature* **519**, 229-232, doi:10.1038/nature14103 PMID - 25517100 (2015).

27 Yoshimura, Y. & Callaway, E. M. Fine-scale specificity of cortical networks depends on inhibitory cell type and connectivity. *Nature Neuroscience* **8**, 1552-1559, doi:10.1038/nn1565 PMID - 16222228 (2005).

28 Grubb, M. S. & Thompson, I. D. Quantitative Characterization of Visual Response Properties in the Mouse Dorsal Lateral Geniculate Nucleus. *Journal of Neurophysiology* **90**, 3594-3607, doi:10.1152/jn.00699.2003 (2003).

29 Zhao, X., Chen, H., Liu, X. & Cang, J. Orientation-selective Responses in the Mouse Lateral Geniculate Nucleus. **33**, 12751-12763, doi:10.1523/JNEUROSCI.0095-13.2013 (2013).

30 Suresh, V. *et al.* Synaptic contributions to receptive field structure and response properties in the rodent lateral geniculate nucleus of the thalamus. *Journal of Neuroscience* **36**, 10949-10963, doi:10.1523/JNEUROSCI.1045-16.2016 (2016).

31 Tang, J., Jimenez, S. C. A., Chakraborty, S. & Schultz, S. R. Visual receptive field properties of neurons in the mouse lateral geniculate nucleus. *PLoS ONE* **11**, 1-34, doi:10.1371/journal.pone.0146017 (2016).

32 Sun, W., Tan, Z., Mensh, B. D. & Ji, N. Thalamus provides layer 4 of primary visual cortex with orientation- and direction-tuned inputs. *Nature Neuroscience* **19**, 308-315, doi:10.1038/nn.4196 PMID - 26691829 (2016).

33 Cruz-Martín, A. *et al.* A dedicated circuit links direction-selective retinal ganglion cells to the primary visual cortex. *Nature* **507**, 358-361, doi:10.1038/nature12989 PMID - 24572358 (2014).

34 Ringach, D. in *The New VisualNeurosciences, MA:, 2013.* (eds JS Werner & LM Chalupa) (MIT Press, 2013).

35 Dhande, O. S., Stafford, B. K., Lim, J.-H. A. & Huberman, A. D. Contributions of Retinal Ganglion Cells to Subcortical Visual Processing and Behaviors. *Annual Review of Vision Science* **1**, 291-328, doi:10.1146/annurev-vision-082114-035502 (2015).

36 Román Rosón, M. *et al.* Mouse dLGN Receives Functional Input from a Diverse Population of Retinal Ganglion Cells with Limited Convergence. *Neuron* **102**, 462-476.e468, doi:10.1016/j.neuron.2019.01.040 (2019).

37 Marshel, J. H., Garrett, M. E., Nauhaus, I. & Callaway, E. M. Functional specialization of seven mouse visual cortical areas. *Neuron* **72**, 1040-1054, doi:10.1016/j.neuron.2011.12.004 (2011).

38 Liang, L. *et al.* A Fine-Scale Functional Logic to Convergence from Retina to Thalamus. *Cell* **173**, 1343-1355.e1324, doi:10.1016/j.cell.2018.04.041 (2018).

39 Wei, W. Neural mechanisms of motion processing in the mammalian retina. *Annual Review of Vision Science* **4**, 165-192, doi:10.1146/annurev-vision-091517-034048 (2018).

40 Rochefort, N. L. *et al.* Development of direction selectivity in mouse cortical neurons. *Neuron* **71**, 425-432, doi:10.1016/j.neuron.2011.06.013 (2011).

41 Liang, L. *et al.* Retinal Inputs to the Thalamus Are Selectively Gated by Arousal. *Current Biology* **30**, 3923-3934.e3929, doi:10.1016/j.cub.2020.07.065 (2020).

42 Hillier, D. *et al.* Causal evidence for retina-dependent and -independent visual motion computations in mouse cortex. *Nature Neuroscience* **20**, 960-968, doi:10.1038/nn.4566 PMID - 28530661 (2017).

43 Harris, K. D. & Mrsic-Flogel, T. D. Cortical connectivity and sensory coding. *Nature* **503**, 51-58, doi:10.1038/nature12654 PMID - 24201278 (2013).

44 Heeger, D. J., Boynton, G. M., Demb, J. B., Seidemann, E. & Newsome, W. T. Motion Opponency in Visual Cortex. *Journal of Neuroscience* **19**, 7162-7174, doi:10.1523/jneurosci.19-16-07162.1999 PMID - 10436069 (1999).

45 Ringach, D. L. Haphazard wiring of simple receptive fields and orientation columns in visual cortex. *Journal of neurophysiology* **92**, 468-476, doi:10.1152/jn.01202.2003 (2004).

46 Lien, A. D. & Scanziani, M. Tuned thalamic excitation is amplified by visual cortical circuits. *Nature Neuroscience* **16**, 1315-1323, doi:10.1038/nn.3488 PMID - 23933748 (2013).

47 Krieger, B., Qiao, M., Rousso, D. L., Sanes, J. R. & Meister, M. Four alpha ganglion cell types in mouse retina: Function, structure, and molecular signatures. *PLOS ONE* **12**, e0180091, doi:10.1371/journal.pone.0180091 PMID - 28753612 (2017).

48 Mauss, A. S., Vlasits, A., Borst, A. & Feller, M. Visual Circuits for Direction Selectivity. *Annual Review of Neuroscience* **40**, 1-20, doi:10.1146/annurev-neuro-072116-031335 PMID - 28418757 (2016).

49 Borst, A. & Helmstaedter, M. Common circuit design in fly and mammalian motion vision. *Nature Neuroscience* **18**, 1067-1076, doi:10.1038/nn.4050 PMID - 26120965 (2015).

50 Borst, A. & Euler, T. Seeing Things in Motion: Models, Circuits, and Mechanisms. *Neuron* **71**, 974-994, doi:10.1016/j.neuron.2011.08.031 PMID - 21943597 (2011).

51 Lien, A. D. & Scanziani, M. Cortical direction selectivity emerges at convergence of thalamic synapses. *Nature* **558**, 80-86, doi:10.1038/s41586-018-0148-5 PMID - 29795349 (2018).

52 Ringach, D. L. You get what you get and you don't get upset. *Nature neuroscience* **14**, 123-124, doi:10.1038/nn0211-123 (2011).

53 Mazade, R. & Alonso, J. M. Thalamocortical processing in vision. *Visual Neuroscience* **34**, E007-E007, doi:10.1017/S0952523817000049 (2017).

54 Kondo, S. & Ohki, K. Laminar differences in the orientation selectivity of geniculate afferents in mouse primary visual cortex. *Nature Neuroscience* **19**, 316-319, doi:10.1038/nn.4215 PMID - 26691830 (2016).

55 Malone, B. J. & Ringach, D. L. Dynamics of Tuning in the Fourier Domain. *Journal of Neurophysiology* **100**, 239-248, doi:10.1152/jn.90273.2008 PMID - 18480369 (2008).

56 Ringach, D. L., Sapiro, G. & Shapley, R. A subspace reverse-correlation technique for the study of visual neurons. *Vision Research* **37**, 2455-2464, doi:10.1016/S0042-6989(96)00247-7 (1997).

57 Ringach, D. L. *et al.* Spatial clustering of tuning in mouse primary visual cortex. *Nature communications* **7**, 12270-12270, doi:10.1038/ncomms12270 (2016).

58 Berens, P. *et al.* Community-based benchmarking improves spike rate inference from two-photon calcium imaging data. *PLOS Computational Biology* **14**, e1006157, doi:10.1371/journal.pcbi.1006157 PMID - 29782491 (2018).